

## CHARACTERISTICS AND EFFICACY OF ULTRAFAST LASER PULSES FOR BIOMEDICAL APPLICATIONS

Bibi Safia Haq<sup>1,2</sup>, Shahnaz Attaullah<sup>3</sup>, Abdul Shakoor<sup>4</sup>, Hidayat Ullah Khan<sup>5</sup>, Khan Alam<sup>5</sup>, Kausar Shaheen<sup>1</sup>

### ABSTRACT

*For the fabrication of three dimensional cell scaffolds, femtosecond laser irradiation at 800nm was used for biomedical applications. The femtosecond laser system was also used to fabricate a bricks and mortar structure in keratin films to investigate skin structures for different cream absorption. The laser characterised here is Spectra Physics, Hurricane X. This is a complex laser system consisting of a seed laser and a regenerative amplifier. It is important to have knowledge of these characteristics to be able to predict the transport of the beam through various optical elements and also to analyse the subsequent interaction with materials. The whole optical intensity profile in two dimensional space of a laser beam i.e. across the beam radius and its detailed shape has been measured and it has been demonstrated that Ti: sapphire laser system has the ability to fabricate three dimensional structures for bio-medical applications. Tissue scaffolds have been prepared with different pore sizes suitable for application in different living tissues. Polymerisation based on a direct write system to build up solid polymeric material for the fabrication of three dimensional cell scaffolds can be achieved. By tailoring the optical system and making use of a relatively weak absorption cross-section we have been able to manufacture deep structures in a single pass of the laser light.*

**KEYWORDS:** *Ultrafast pulses, femtosecond laser, three dimensional structures, cell scaffold, biomedical applications*

### INTRODUCTION

This work sets out to study the use of lasers in material structuring for bio-medical applications. We have chosen the term “biomedical” as opposed to “biological” or “medical” to encompass the field of applied research that contributes to the development of new treatments rather than clinical trials. In this way, the study explores the use of lasers in such treatments or in the production of structures required for research into new procedures.

Laser processing can generate structures on the micron scale (and in some cases, nanometre scale) in metals, dielectrics and semiconductors. In order to form surfaces and volumes that are suitable for biomedical applications, the action of the laser radiation can be subtractive or additive. An increasingly common ablative medical procedure is corneal sculpting. In most cases this can be considered a bulk material interaction. In additive patterning, the surface relief is formed by depositing material, normally on a support or substrate. In the bio-medical arena, direct write techniques have been used to carefully deposit sensitive materials that are damaged by other techniques. Such methods provide an ideal way to transfer chemically, physically and biologically complex

materials by allowing the laser interaction to propel the majority of the desired material to the substrate without harm. Biomaterials such as proteins, bacteria, DNA and stem cells can be deposited in a similar manner without compromising the viability of these delicate structures. Liquids can also be transferred by laser-based techniques; direct writing has been used to transfer water-based solutions of proteins and a single cell suspension with small volume droplets of the order of 10fL successfully onto solid substrates<sup>1</sup>. In this way, laser direct write transfer is an exciting tool for applications such as manufacturing of miniaturized biosensors, implantable drug delivery systems, tissue engineering studies and placement of cells<sup>1</sup>.

Two-photon absorption polymerization processes (TPP) can be used to fabricate 3D micron size structures with high spatial resolution. The laser systems that have been used for biomedical applications in this work was a femtosecond titanium sapphire (Ti: sapphire) laser. A Ti: sapphire lasers having ultrahigh peak powers with approximately 100 femtosecond (fs) pulse width, and a wavelength of 800nm which is close to the half of the wavelength of polymerisation is used to control the polymerisation threshold energy<sup>2</sup>. Due to the smaller heat

<sup>1</sup> Department of Physics, JCW, University of Peshawar, Khyber Pakhtunehwa, Pakistan

<sup>2</sup> Department of Physics & Materials, University of Hull, Hull, HU6 7RX, United Kingdom

<sup>3</sup> Department of Chemistry, JCW, University of Peshawar, Khyber Pakhtunehwa, Pakistan

<sup>4</sup> Department of Materials, SAACME, Loughborough University, LE11 3TU, United Kingdom

<sup>5</sup> Department of Physics University of Peshawar, Khyber Pakhtunehwa, Pakistan

affected zone and reduced plasma screening effect, the femtosecond laser has certain advantages over longer pulses<sup>3</sup>. Precise laser machining and 3D micro and nano structure fabrication can be achieved by using point-by-point processing with the femtosecond laser system. The femtosecond laser system was also used to fabricate bricks and mortar structure in keratin films to investigate skin structures for different cream absorption.

Laser beams can have varying degrees of monochromaticity, can be temporally and spatially coherent and may propagate with a variety of irradiance profiles. It is important to have knowledge of these characteristics to be able to predict the transport of the beam through various optical elements and also to analyse the subsequent interaction with materials. Here, measurements have been made of the beam parameters and a summary of the laser performance given for the Ti: sapphire laser systems. We describe the laser systems used and quantify their performance via their output characteristics.

## THE FEMTOSECOND TITANIUM SAPPHIRE LASER CHARACTERISTICS

The laser characterised here is a Spectra Physics, Hurricane X. This is a complex laser system consisting of a seed laser and a regenerative amplifier. Chirped pulse amplification is utilised to avoid optical damage to the amplifier; the seed pulses are stretched in time, amplified, and then compressed back to nearly their original duration. The seed laser is a mode-locked Ti: sapphire oscillator pumped by a frequency doubled, diode-laser pumped, Nd: YVO4 laser. This system gives ~100fs duration pulses at 80MHz repetition rate. As the regenerative amplifier is excited at 1 kHz by a diode-laser pumped, frequency doubled, Nd: YLF laser (527nm), seed pulses are selected and introduced into the amplifier by a Pockels cell at this lower repetition rate. A second Pockels cell allows the timing of the exit of the amplified pulse relative to the Nd:YLF laser excitation pulse (~100ns in duration) to be altered and therefore the output energy of the femtosecond pulse. However, leaving the pulse circulating in the amplifier leads to pulse broadening and so it is often better to time the switching of the Pockels cell so that it coincides with the peak of the gain and then attenuate the beam outside of the laser if less energy is required. In this way, the Hurricane X system can nominally deliver

1mJ pulse energies in 100fs pulses at 800nm wavelength with a frequency of 1 kHz. This has 1W average power but each pulse has a peak power of ~  $10^{13}$ W (10TW). Measurements of the laser characteristics are given in the following sections.

## RESULTS

### Beam profile

The whole optical intensity profile in two dimensional space of a laser beam i.e. across the beam radius and its detailed shape can be measured with the help of a diagnostic device known as a beam profiler (or beam analyser). The beam analyser used here is based on a silicon CCD sensor (OPHIR Beam Star profiler V-PCI), with a sensor size of 6.4 mm x 4.8mm corresponding to 320 x 240 pixels in both dimensions respectively. This device has useful sensitivity in the near infrared and visible spectral regions. The pixel size and hence the spatial resolution, is of the order of 5 $\mu$ m. Different parameters such as beam radius, beam position, ellipticity and Gaussian fits are displayed via software on a PC to which the CCD array is connected.

As the CCD sensor is very sensitive to light, it was necessary to attenuate the beam to prevent saturation. This was achieved by placing the beam profiler behind a dielectric beam turning mirror which had a nominal reflectivity of approaching 100%. The distance from the laser output to the CCD was of the order of 2m. As the sensor has a fixed frame rate of 25Hz it is difficult to synchronise the data capture with the arrival of a laser pulse. Therefore, the laser was allowed to run at 1kHz and the software adjusted to reject blank frames. In this way the figures shown represent a typical frame that contained pulse data. Figure 1 shows the measured vertical and horizontal profiles through the centre of the beam together with Gaussian beam fits at an emission wavelength of 800nm. In Figure 2 the 2-D profile is given with the highest intensity coloured yellow and the background light level blue. Table 1 summarises the beam diameters in the different directions as measured using the raw data or the Gaussian fits. The CCD pixel values are proportional to the irradiance and therefore it is appropriate to use the  $1/e^2$  point to evaluate the beam width (diameter); this is given as the 13.5% width. For completeness the  $1/e$  width is also given which represents

the equivalent beam size in electric field. It is also possible to see<sup>4,6</sup> in figure 2 small dark spots with concentric rings. These were found to move with the CCD sensor and are therefore thought to be associated with dust and not intrinsic to the beam itself. The concentric rings illustrate the coherence of the beam as these are thought to be Newton's rings formed from the scattered light. The beam can also be seen to be slightly wider in the horizontal direction than the vertical. Defining the ellipticity of the beam as  $\sqrt{\frac{major^2 - minor^2}{major^2}}$  gives a value of 0.56 for this beam.

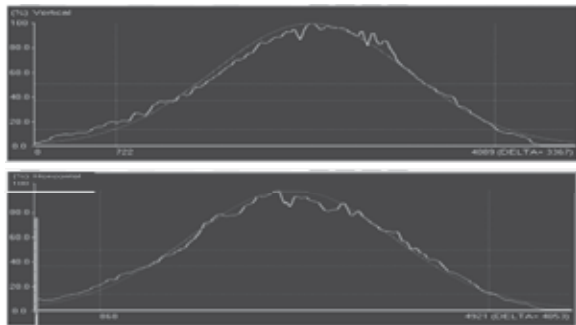


**Figure 1. Vertical and horizontal line profiles through the centre of the beam. The raw data is shown in white together with a Gaussian fit in red. The laser was operating at 800nm wavelength and 1kHz. The intensity was attenuated by placing the sensor behind a dielectric turning mirror of near 100% reflectivity.**

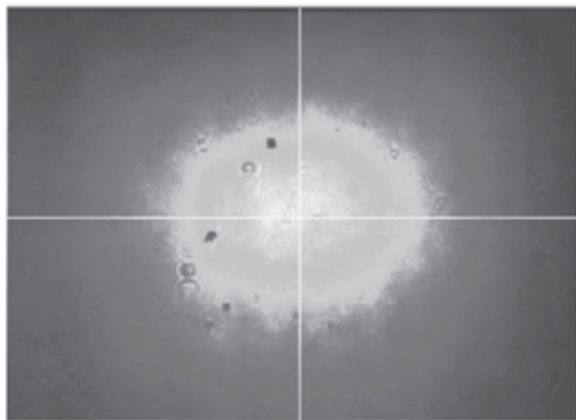


**Figure 2. Colour coded 2-D intensity pattern showing in white the position that the line profiles in Figure 1 were measured through. Yellow areas are high intensity with blue regions being the background level.**

It is possible to use the high intensity 800nm wavelength beam to create 400nm wavelength pulses via second harmonic generation. A commercial system from Spectra Physics was used for this purpose. The conversion efficiency, coupled with the transmission loss of the optical elements gave approximately 20% of the input power at 800nm as 400nm output. Figure 3 shows the vertical and horizontal Gaussian beam fits for the 400nm wavelength beam approximately 30cm after the output of the second harmonic generator. The 2D view and 3D view of the shape of this beam is shown in Figure 4(a) and Figure 4(b) respectively while Table 2 Figure 4 (a) Beam shape of the femtosecond laser beam at 400nm wavelength generated using the frequency doubling crystal (2D view) (b) 3D structure of the laser beam at 400nm wavelength measured with the CCD sensor.

indicates the vertical and horizontal beam sizes at 400nm. It can be seen that the 400nm output is smaller in size than the 800nm input. This can be attributed to two reasons; the second harmonic generation is controlled by the irradiance and so the wings of the Gaussian distribution will not undergo conversion and also, the second harmonic generator includes focussing and collimating optics that may change the beam divergence. The beam can also be seen to contain fewer fluctuations in irradiance (i.e. it is “smoother”) and as a result has a better correlation to the Gaussian fit<sup>5,6</sup> (Figure 3). However, the 400nm wavelength beam pointing stability was not as good as the 800nm output from the laser and could be seen to move from the centre of the CCD by approximately 100µm from pulse-to-pulse.

**DIVERGENCE OF THE BEAM**

The lowest order Gaussian beam is characterized by the spot size  $\omega_0$  known as the beam waist is given by the equation

where  $f$  is the focal length of the lens,  $\lambda$  is the

$$\omega_0 = \frac{f \lambda}{\pi \omega_L} \tag{1}$$

wavelength of the laser beam and  $\omega_L$  is the size of the beam entering the lens. The beam size as a function of distance,  $z$ , can be found from equation (2). Here, the beam size  $\omega(z)$  is related to the beam waist,  $\omega_0$ , by the ratio  $z/zR$  <sup>5</sup>.

**Table 1. Horizontal and Vertical beam diameter of the femtosecond laser beam at 800nm wavelength.**

Femtosecond laser pulses at 800 nm wavelength	Horizontal		Vertical	
	Beam	Gaussian	Beam	Gaussian
Width (µm) 1/e (36.5%)	3145.18	3020.16	2498.83	2487.41
Width (µm) 1/e2 (13.5%)	4248.25	4257.11	3726.30	3506.16

**Table 2. Horizontal and Vertical beam diameter of the femtosecond laser beam at 400nm wavelength.**

Femtosecond laser pulses at 400 nm wavelength	Horizontal		Vertical	
	Beam	Gaussian	Beam	Gaussian
Width (µm) 1/e (36.5%)	610.69	605.14	473.95	473.38
Width (µm) 1/e2 (13.5%)	840.18	852.99	657.25	667.25

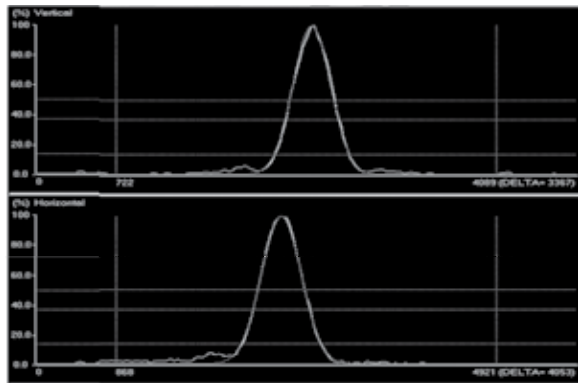


**Figure 3. Vertical and horizontal line profiles through the centre of the beam. The raw data is shown in white together with a Gaussian fit in red. The laser has been frequency doubled to a wavelength of 400nm wavelength. The repetition rate was 1kHz.**



**Figure 4. (a) Beam shape of the femtosecond laser beam at 400nm wavelength generated using the frequency doubling crystal (2D view) (b) 3D structure of the laser beam at 400nm wavelength measured with the CCD sensor.**

Due to diffraction spreading, an ideal Gaussian beam

$$\omega(z) = \omega_0 \sqrt{1 + \left(\frac{z}{z_R}\right)^2} \quad (2)$$

expands as it propagates away from the waist region as

shown in Figure 5. It remains approximately collimated over a short distance in the near field and diverges in the far field. The distance over which the beam travels from the waist before the beam diameter increases by  $\sqrt{2}$  (i.e. its area doubles) is given simply by the parameter

In terms of the Rayleigh range, the wave front radius

$$z = z_R = \frac{\pi\omega_0^2}{\lambda} = \text{Rayleigh range}$$

of curvature can be written as,

Substituting the value of the Rayleigh range, equation (2) can be written as

$$R(z) = z \left[ 1 + \left(\frac{z_R}{z}\right)^2 \right]$$

Here z is the distance propagated from the focal plane

$$\omega(z) = \omega_0 \left[ 1 + \left(\frac{\lambda z}{\pi\omega_0^2}\right)^2 \right]^{1/2} \quad (3)$$

and  $\lambda$  is wavelength,  $\omega_0$  is the radius of the 1/e electric field. For large z, R(z) asymptotically approaches z and  $\omega(z)$  approaches the value<sup>6</sup>

$$\omega(z) = \frac{\lambda z}{\pi\omega_0} \quad (4)$$

where z is presumed to be much larger than  $\pi\omega_0^2/\lambda$  so that the 1/e electric field contour (1/e2 in irradiance) approaches a cone of angular size

$$\theta = \frac{\omega(z)}{z} = \frac{\lambda}{\pi\omega_0} \quad (5)$$

The Rayleigh range is the dividing line between near field divergence and mid- range divergence. Far field

divergence must be measured at a point  $>zR$ .

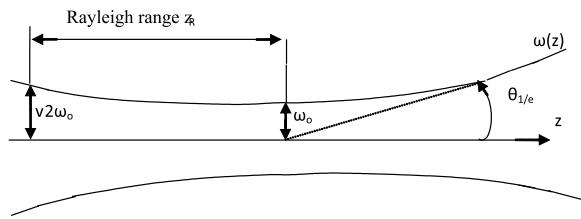


**Figure 5.** Here the approximately collimated waist region of the Gaussian beam is shown together with the Rayleigh range.

The beam diameter of the train of femtosecond laser pulses was measured with the help of the CCD system placed at different positions along the optical path. This data is plotted in Figure 6. The graph indicates that at this point in the optical path the beam is slowly converging and that the laser system, with its series of cavities (one for the seed laser and another for the regenerative amplifier) and stretcher/compressor (which includes a focussing mirror) results in a waist outside of the enclosure. The slightly elliptical nature of the beam can be seen as the horizontal axis has a larger diameter but this does not result in an appreciable difference between the horizontal and vertical divergence angles as the lines of best fit are quite parallel (Figure 6). In order to quantify the beam divergence, a lens was placed in the beam path (plano-convex, focal length 300mm) and measurements taken of the beam diameter as a function of distance before and after the geometric focal point. It was not possible to measure the focal spot size directly as the irradiance was too high and damage to the CCD would result. In addition, as the beam waist predicted from equation 1 is approximately  $20\mu\text{m}$  in diameter and the CCD pixel size is  $\sim 12\mu\text{m}$ , there is insufficient resolution to observe it accurately. By interpolating the data back towards the focal point the beam waist can be inferred and the divergence taken as the ratio of this size to the focal length.

Horizontal and vertical beam diameters were plotted against distance as shown in Figure 7 and Figure 8 respectively. The graph obtained shows that the size of the beam decreases towards the focus and is smallest near 275mm which is close to the geometrical focus of

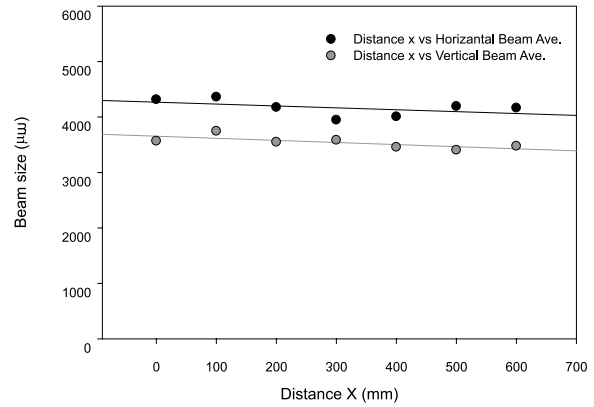


**Figure 6.** Graph between the distance and beam size without using lens

the lens. This is in accordance with the fact that when a beam is focused by the ideal lens, a slight shift in position between the geometrical focus of the lens and the actual waist of the focused Gaussian beam is always present<sup>7</sup>. The theoretically calculated values of  $\omega(z)$  were plotted against distance and shown in the same Figure 7 and Figure 8 for horizontal and vertical beam diameters. Experimental data and theoretically calculated data for both horizontal and vertical beam diameters do not show symmetry after focus point. This is due to high irradiance at focal position which changes the refractive index and disturbs propagation of the beam beyond the focal point.

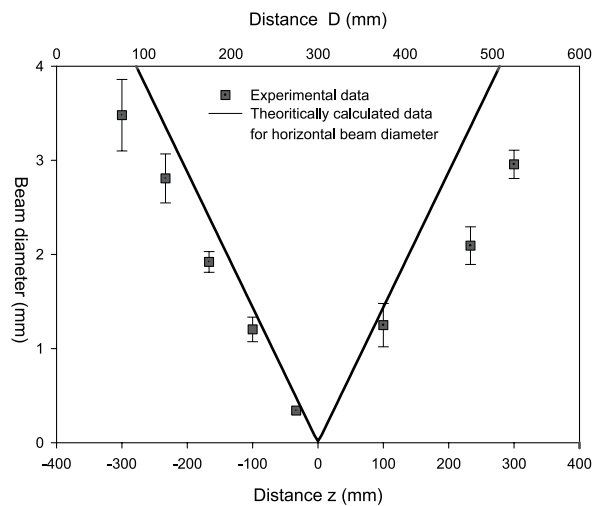


**Figure 7.** shows experimental data for the beam size as a function of distance using a 300mm lens for horizontal beam diameters. The calculated beam diameter  $\omega(z)$  vs. distance is also plotted.

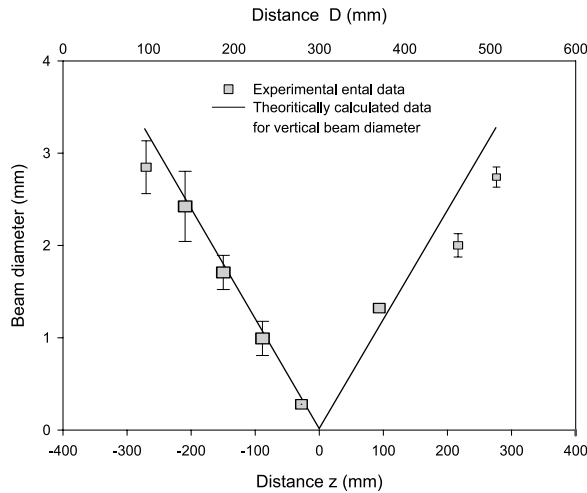


**Figure 8.** show experimental data for the beam size as a function of distance using a 300mm lens for vertical beam diameters. The calculated beam diameter  $\omega(z)$  vs. distance is also plotted.

The experimental values obtained for horizontal and vertical beam waists were found to be  $17.7\mu\text{m}$  and  $21.4\mu\text{m}$  respectively. The fit to the expected curve is not that good and the beam quality should be considered to explain this departure. The next section discusses this.

### M<sup>2</sup> FACTOR

The M<sup>2</sup> Factor is a measure of the beam quality. M<sup>2</sup> is a numerical quantity which in the far field region compares the focused diameter of a pure Gaussian beam with the diameter of the real focused beam. The concept of M<sup>2</sup> is useful in measuring the mode quality of a laser beam. Knowing M<sup>2</sup>, it becomes possible to align laser mirrors or adjust the aperture of the beam to produce the desired quality. It is related to the half angle beam divergence given by

$$\theta = M^2 \frac{\lambda}{\pi\omega_0} \tag{6}$$

For a pure Gaussian beam the M<sup>2</sup> value is 1, and higher values indicate poorer quality (higher mode content) beams<sup>8,9</sup>. The propagation equations for  $\omega(z)$  and  $R(z)$  of a mixed mode beam are given by

$$\omega(z) = \omega_0 \left[ 1 + \left( \frac{M^2\lambda z}{\pi\omega_0^2} \right)^2 \right]^{1/2} \tag{7}$$

Using the experimental data from the previous section

$$R(z) = z \left[ 1 + \left( \frac{\pi\omega_0^2}{M^2\lambda z} \right)^2 \right] \tag{8}$$

and by choosing suitable values for M<sup>2</sup> and substituting into equation (7), theoretical values  $\omega(z)$  have been calculated. Experimental and theoretically calculated data

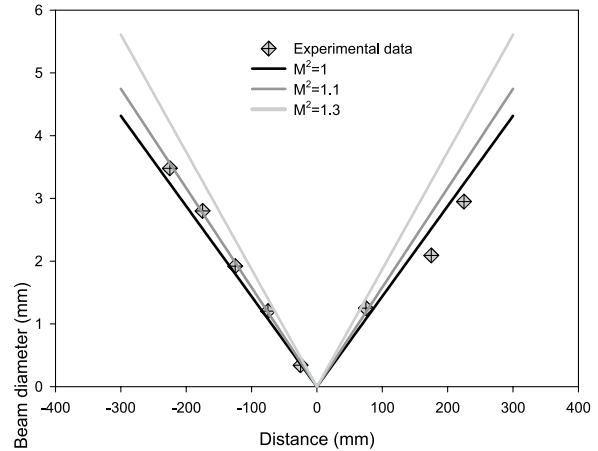


**Figure 9.** Comparison of the experimental and theoretical data for M<sup>2</sup> values for horizontal beam diameter

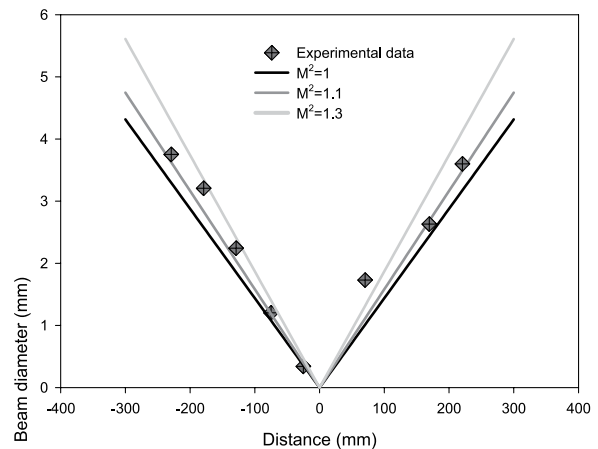


**Figure 10.** Comparison of the theoretical and experimental data for different M<sup>2</sup> values for vertical beam diameter

can be compared as shown in Figure 9 for the horizontal beam diameter and in Figure 10 for the vertical beam diameter.

It can be seen that the horizontal data has a good fit to M<sup>2</sup> = 1.1 before the focal point. This agrees with manufacturer’s data. After the focal point the correlation

is poorer. This may be partly due to refractive index disturbances in the air caused by the much higher intensity in the region of the focus even though the beam had been attenuated and no visible breakdown was observed.

### WAVELENGTH

The wavelength of the femtosecond laser beam was measured with the help of a computer controlled spectrometer type S2000 visible to NIR (Near Infra red Radiation) manufactured by Ocean Optics with serial no. HR2A0734. This system has a resolution of 0.5nm which was deemed sufficient as the output of the femtosecond laser was expected to be relatively broad. Scattered light from the laser beam was delivered to the spectrometer by a multimode fibre optic and an integration time of 30ms was used to improve the signal to noise ratio and also to average over several laser pulses. The calibration was checked using a HeNe laser operating at 632.8nm and the spectrometer was found to be reading 2nm too long. This has been corrected for in the data shown. The corrected wavelength measured was 802nm and the full

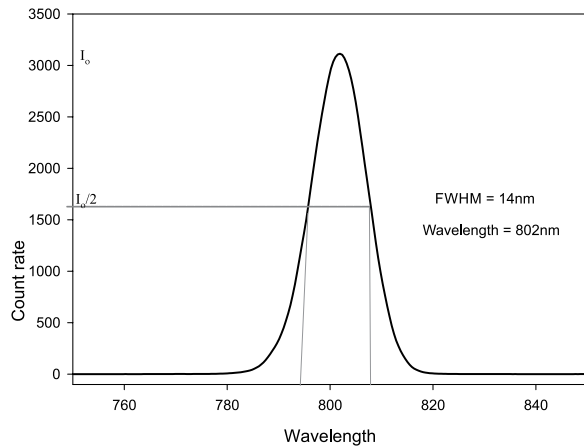


**Figure 11. Fundamental emission of the femtosecond laser at 802nm wavelength measured using a fibre coupled spectrometer.**

width at half maximum was 13nm as shown in Figure 11. This is slightly longer than the expected 800nm output although the seed laser does have a scanning function with a range 790 – 810nm. The scanning control software reported the wavelength as being set to 800nm.

Using the fundamental output of the laser, a second harmonic generator was used to give an output around

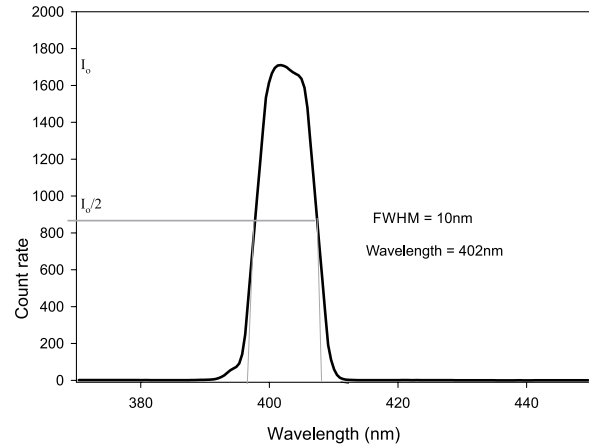


**Figure 12. Wavelength spectrum of the frequency doubled femtosecond laser beam at 402nm.**

400nm and scattered light was again measured with the fibre coupled spectrometer. The same integration time of 30ms was used. The wavelength of femtosecond laser after passing through frequency doubling crystal was measured as 402nm and the full width and half maximum was 10nm as shown in Figure 12.

### 3.5 PULSE DURATION

The minimum duration of an individual pulse from the laser is related to the bandwidth of the output and hence the data from the above section can be used to estimate the shortest pulse that could be expected. A so-called bandwidth limited optical pulse or one reaching the Fourier transform limit has the lower limit for pulse duration that is possible for the optical bandwidth of that pulse. A pulse at this limit is called transform limited. To calculate the transform limited pulse the minimum time-bandwidth product should be calculated when there is no chirp. The Fourier transform of a Gaussian pulse is a Gaussian function and the spectral width and the duration of a pulse are related quantities. From the uncertainty principle we know that

$$\Delta t \Delta E \geq \frac{\hbar}{2}$$

As

$$E = h\nu = \hbar\omega$$

$$\text{Therefore } \Delta t \Delta\omega \geq \frac{1}{2} \tag{9}$$

The equality in equation (9) is only reached for pulses that have an electric field envelope in time that is Gaussian. Making this assumption but using a more convenient width measurement at the half maximum point (FWHM) and frequency (rather than angular frequency) changes the constant from 0.5 to 0.441<sup>9</sup>. Equation (9) is now written as,

$$\Delta t \Delta \nu \geq 0.441 \quad (10)$$

Other pulse shapes require different constants but here we continue with the Gaussian assumption as the autocorrelator used to measure the duration also makes this assumption.

The emission width measured in the previous section was 14nm at a central wavelength of 802nm. This corresponds to a frequency bandwidth of 6.5x10<sup>12</sup> Hz and therefore minimum pulse duration of 68fs.

Current technology for measuring optical pulses directly is limited by the response time of a photo detector and oscilloscope combination. For a repetitive waveform this can be as fast as 10's of ps. For example, Hamamatsu offer a metal-semiconductor-metal (MSM) photodiode with a rise-time of 30ps and LeCroy can supply oscilloscopes with 100GHz bandwidth. However, this is still much longer than the transform limited pulse calculated above. Therefore an indirect method must be used. Streak cameras are one option but here an optical autocorrelator has been used. There are also techniques such as FROG (frequency resolved optical gating) or SPIDER (spectral phase interferometry for direct electric field reconstruction)<sup>10</sup> that can be used to obtain much more information on the real pulse shape in time but their complexity and cost precluded their use here.

Fundamental wavelength laser pulses were sampled by using a flat glass plate to direct ~5% of the main pulse train into an APE Pulse Check autocorrelator (APE ser.03/3A211). It was ensured that only the reflection from the front face of the plate was allowed to enter the device so that a double pulse was not measured. Attenuation of the main pulse train was additionally required and was achieved using neutral density filters. The optical path length of the stretcher-compressor can be adjusted using a motorised stage and this was optimised for the shortest output pulse. In addition, the alignment

of the regenerative amplifier together with the Pockel cell timing affects the gain build-up time and therefore how long the seed pulse circulates in the system. Due to dispersion, this has an effect on the pulse duration as well<sup>11</sup>. A cleaned and freshly aligned system (i.e. just after manufacturer servicing) was measured as having a pulse duration of ~120fs. As the system becomes lousy (e.g. absorption in the stretcher-compressor section) and less well aligned, the pulse extends in time. Consequently, brief re-alignment, as achievable for daily use, gave usual pulse durations in excess of this and measurement at the start of each experiment was required. It will be seen that the pulse durations used throughout the rest of the thesis broadly fall into an interval of not being shorter than 120fs and not exceeding 180fs with the most prevalent timescale being ~160fs<sup>11</sup>.

## FABRICATION OF 3D STRUCTURES

A desired tissue shape and a porous interconnected micro-architecture structure are required for biodegradable and biocompatible scaffolds for tissue engineering. In order to encourage cells to build an artificial living tissue, an appropriate environment exactly resembling that of a particular tissue type has to be created. Porous scaffold geometries are required to have high surface area for initial cell attachment and a specific micro-scale pore size depending on cell/tissue types. The pore sizes depend on the desired cell/tissue type and values ranging from ~5µm to hundreds of microns are reported according to the cell/tissue types used in various research<sup>12</sup>. 2D and 3D environments are required for the cell type to preserve tissue specific features. TPP techniques used with the right material allows the fabrication of 3D scaffolds with precise control over geometry to reproduce microcellular environments and provide control over cell organisation inside the scaffold and over the cell interaction<sup>13</sup>.

A femtosecond laser beam of wavelength 800 nm at 420µW power having pulse duration of 180fs with repetition rate of 1 kHz was made incident on the sample with a writing speed of 1mm/min. The sample was analyzed with a Leica DM LM optical microscope which showed the presence of a scaffold covered with liquid resin. The scaffolds obtained were rinsed many times in deionised water to remove the liquid EBPADMA from the slide to get cell scaffolds as shown in Figure 13 (a) and (b). The scaffold obtained contains pores of

approximately  $47\mu\text{m}$ , a pore size suitable for the liver tissue<sup>12</sup>. The size of the ridges between these large sized pores was approximately  $37\mu\text{m}$  wide due to fabrication at low speed i.e., at  $v=1\text{mm}/\text{min}$ .

To investigate effects of cream on human skin, model skin structure has been fabricated using laser processing of keratin. 250nm and 70 nm thick keratin films were ablated to fabricate a bricks and mortar pattern structure as shown in Figure 13(c). A near infrared mode-locked Ti: Sapphire femtosecond laser of wavelength 800nm with 160fs pulse duration and 1 kHz repetition rate has been used for the fabrication of structure.

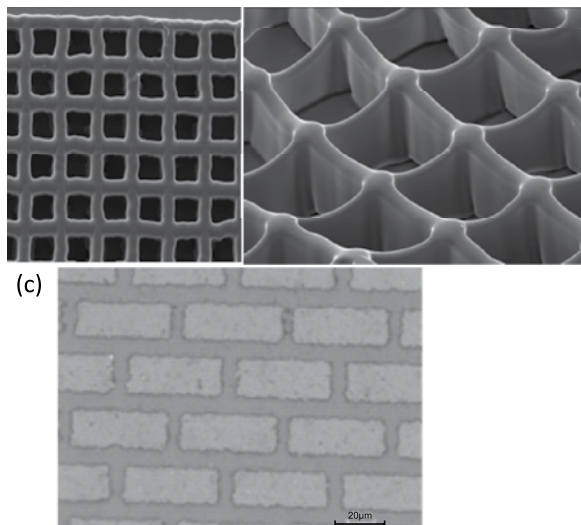


**Figure 13. 3D structures for biomedical applications (a) and (b) show cell scaffold with different pore size. (c) bricks and mortar pattern in keratin film.**

## CONCLUSIONS:

This research was aimed to investigate the laser characteristics for the fabrication of cell scaffolds for tissue engineering, and to perform studies of material ablation for medical applications. It has been demonstrated that laser systems that have been employed in this study have the ability to fabricate tissue scaffolds with different pore sizes suitable for application in different living tissues. Three dimensional micrometer size structures were polymerised on glass substrates using liquid resin Ethoxylated Bisphenol A Dimethacrylate. By moving the laser focus through the resin in three dimensions, 3D structures of different shapes and different pore sizes

were fabricated. The primary function of the scaffold structure is to provide a 3D environment for the cells to migrate and to proliferate.

A bricks and mortar pattern in keratin films has been fabricated using femtosecond laser system at 800nm and 400nm wavelengths. Due to the very low ablation threshold of keratin, femtosecond laser systems are practical for laser processing of proteins.

## REFERENCES

1. Sugioka, K., Meunier, M. and Pique, A., 2011. "Laser Precision Micro Fabrication". 135 ed: Springer.
2. Lee, K. S., Yang, D.Y., Park, S. H. and Kim, R. H., 2006, "Recent developments in the use of two-photon polymerization in precise 2D and 3D microfabrications". *Polymers for advanced technologies* 17: 72-82.
3. Crawford, T.H.R. and Haugen, H.K., 2007. "Sub-wavelength surface structures on silicon irradiated by femtosecond laser pulses at 1300 and 2100 nm wavelength", *Applied Surface Science* 253: 4970-4977.
4. Osborne, P., 2008, "The Mercator Projections". Edinburgh.
5. Siegman, A.E., 1986. "Lasers", 1st ed. United States of America: University Science Books.
6. Siegman, A.E., 1990. "New developments in laser resonator". *Proc. SPIE*.
7. Siegman, A.E., 1993. "Defining, measuring, and optimizing laser beam quality". 2: *Proc. SPIE*.
8. Hall, D.R. and Jackson, P.E., 1989. "The Physics and Technology of Laser Resonators". IOP Publishing Ltd.
9. Rulliere, C., 2006. "Femtosecond Laser Pulses: Principles and Experiments". 2nd ed. New York: Springer.
10. Wolf, E., 2004. "Progress in optics". 46: Elsevier

*Science & Technology.*

11. Diels, J.C. and Rudolf, W., 2006, "Ultrashort Laser Pulse Phenomena". Second Edition ed: Massachusetts, Academic Press.
12. Choi, J.W., Wicker, R., Lee, S.H., Choi, K.-H. Ha, C.S. and Chung, I., 2009. "Fabrication of 3D biocompatible/biodegradable micro-scaffolds using dynamic mask projection micro stereolithography". *Journal of Materials Processing Technology* 209: 5494-5503.
13. Phipps, C., 2007. "Laser ablation and its applications". Santa Fe New Mexico: Springer.